Indian Journal of Pure & Applied Physics
Vol. 55, June 2017, pp. 385-393

# Microstructural characteristics and optical performance of nano-structured thin films of tin oxide

Parveen Jain[a,b], Sukhvir Singh[a]*, Azher Majid Siddiqui[b] & Avanish K Srivastava[a]

[a]Electron and Ion Microscopy Group, CSIR-National Physical Laboratory, New Delhi 110 012, India

[b]Department of Physics, Jamia Millia Islamia, New Delhi 110 025, India

*Received 16 March 2017; revised 4 April 2017; accepted 5 April 2017*

Transparent conducting tin oxide thin films (thickness ~140 nm) have been synthesized by using vacuum evaporation technique under the vacuum of the order of $10^{-6}$ mbar at room temperature. These films have been deposited onto glass and single crystals of KCl substrates and subsequently annealed at different temperatures for varying time periods in high purity oxygen (99.999%) atmosphere to obtain single phase of tin oxide. X-ray diffraction measurements have been carried out on the films deposited onto glass substrates to reveal the phase formation of tin oxide. Secondary ion mass spectrometer (SIMS) and selected area electron diffraction pattern (SAEDP) measurements identify the presence of Sn, SnO and $SnO_2$ phases in the films. Detailed XRD measurements and microstructural features recorded employing SEM, HRTEM, AFM and SIMS have been interpreted in the light of emission bands of these films occurred at 442 nm and 452 nm. The effect of vacuum conditions and annealing on nucleation and growth mechanism of tin oxide thin films has been presented and discussed in detail.

**Keywords:** Tin oxide thin films, Vacuum evaporation, Phase formation, Photoluminescence

## 1 Introduction

In tin-oxygen system two stable oxides of tetragonal modifications SnO and $SnO_2$ are known to exist. $SnO_2$ thin films are widely used in different areas of technical applications. This is a semiconductor material of *n*-type conductivity with the band gap $E_g$ =3.6–4.3 eV and optical transmittance of about 97% in visible and near ultraviolet ranges[1-3]. Tin oxide materials are used in a variety of applications as antistatic films, thin film resistors, and anti reflecting coatings in solar cells. Tin oxides have also been investigated[4-7] as gas sensors for $H_2$, $O_2$, CO, $CO_2$, $NO_x$, $H_2S$, $CH_4$, $C_2H_5OH$, and $C_6H_6$. High electrical conductivity, good chemical stability, high transparency (compared to other metal oxides) in the visible region, and strong physical and chemical interactions with adsorbed species are some important properties of $SnO_2$. $SnO_2$ is also stable thermally in air at up to 500 °C and mechanically in aqueous media. $SnO_2$ thin films can be made easily by standard thin film technologies with a low cost of production, high reliability, and good reproducibility. By chemical route of sol-gel methods, catalysts or doping materials can be added easily to $SnO_2$ to increase sensitivity and selectivity for certain gases. However, surface morphology, chemical composition, defects of tin oxide material, optical properties, and electrical behaviour need to be controlled and understood before $SnO_2$ can be used as gas sensors.

Whatever the methods of preparation of tin dioxide ($SnO_2$) layers, the properties of films are influenced by the surrounding medium (gas, liquidates, etc.), the reagents used (nature, concentration, purity, etc.), the substrate (nature, temperature, etc.) and the annealing of the layers. The complexity of these processes and the various modes of growth of nanocrystals from these layers have led to several techniques of preparation sol–gel[8,9], thermal oxidation[10,11], pyrolysis by spray[12,13] and chemical vapour deposition[14] (CVD). In the present work thermal evaporation technique has been employed to deposit thin films of tin oxides under vacuum of the order of $10^{-6}$ mbar onto the glass and KCl substrates and further annealed at different temperatures for different periods of time in order to synthesize single phase $SnO_2$ thin films. Recently the authors have reported a systematic study of $SnO_2$ thin films synthesized under varied vacuum conditions[15].

*Corresponding author (E-mail: sukhvirster@gmail.com)

## 2 Experimental Details

### 2.1 Synthesis

Tin oxide thin films were synthesized by thermal evaporation at room temperature under vacuum of the order of $6\times10^{-6}$ mbar using high purity tin (99.9999 % pure from M/s Alfa Aiser) as the source material. The thickness of the films was kept around ~140 nm. Liquid $N_2$ trap was used to avoid contamination during the evaporation of the source material. Deposited films were annealed at different temperatures (150 °C, 200 °C, 400 °C, and 500 °C) for different time periods (1 h, 2 h, 5 h, 6 h and 10 h) under high purity oxygen gas atmosphere in order to synthesize good quality single phase tin oxide films. A sketch of the vacuum evaporation unit is shown in Fig. 1. Figure 2 shows the experimental set up to anneal the as deposited films under oxygen atmosphere. A list of experimental details and the structural parameters identified on different thin films are summarized in the Table 1.

### 2.2 Characterization

The detailed study on XRD measurements were carried out on as deposited as well as on annealed films to identify the phase of the tin oxide thin films by using X-ray diffractometer model-Bruker Axes using Cu$K_\alpha$ radiations ($\lambda$ = 1.54178 Å). Photoluminescent (PL) spectrometer model Perkin Elmer LS 55 was used to investigate the photoluminescence properties at the excitation wave length of 350 nm. Surface structure and depth profile measurements of these films were carried out by using time of flight secondary ion mass spectrometer (TOF-SIMS make GmbH Germany). Selected area electron diffraction (SAED) studies were carried out under transmission electron microscope (TEM) model JEM 200CX operated at 160 kV. Thin films were examined for surface morphology by using scanning electron microscope (SEM), Model: Leo EVOMA10. AFM scans were performed using a multimode V; make Veeco Instrument in contact mode with NP20 tips. Effect of annealing temperatures on the transparency of the $SnO_2$ thin films has been displayed as in Fig. 3. It has been observed that the

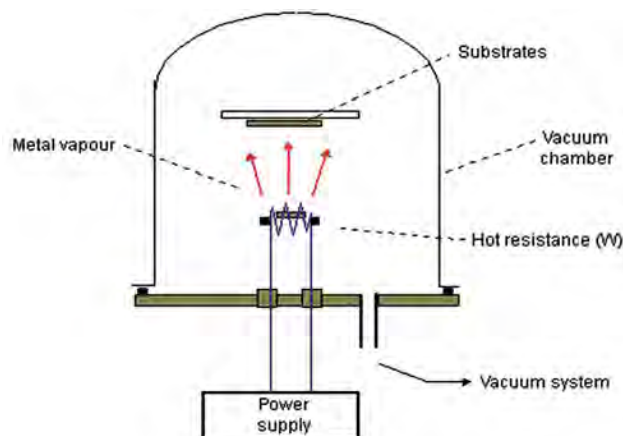


Fig. 1 — A sketch of the vacuum evaporation unit

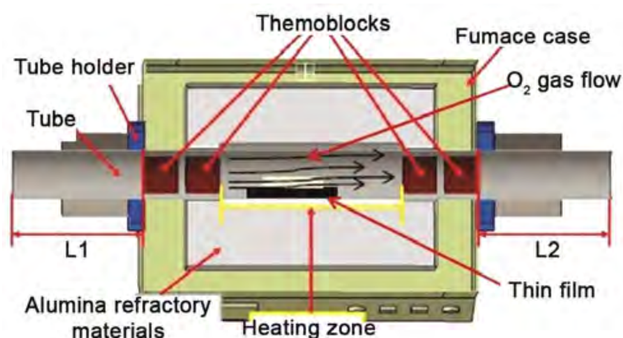


Fig. 2 — A set up for annealing the as deposited films in oxygen atmosphere

Table 1 — Effect of annealing conditions on as deposited Sn thin films under $O_2$ atmosphere

| S. No. | Annealing temperature (°C) | Annealing time (h) | Lattice parameter *a* (Å) | Lattice parameter *c* (Å) | Phase | Structure | JCPDF No | Crystallite size (nm) |
|---|---|---|---|---|---|---|---|---|
| 1 | As deposited | As deposited | 5.831 | 3.181 | Sn | Tetragonal | 86-2265 | 66 |
| 2 | 150 | 2 | 5.831 | 3.181 | Sn | Tetragonal | 86-2265 | 68 |
| 3 | 150 | 5 | 5.831, 3.796 | 3.181, 4.816 | Sn, SnO | Tetragonal | 86-2265, 85-0712 | 46 |
| 4 | 200 | 2 | 5.831 | 3.181 | Sn | Tetragonal | 86-2265 | 66 |
| 5 | 200 | 5 | 5.831, 3.796 | 3.181, 4.816 | Sn, SnO | Tetragonal | 86-2265, 85-0712 | 63 |
| 6 | 400 | 1 | 4.72 | 3.17 | $SnO_2$ | Tetragonal | 03-1116 | 32 |
| 7 | 400 | 6 | 4.72 | 3.17 | $SnO_2$ | Tetragonal | 03-1116 | 25 |
| 8 | 500 | 1 | 4.72 | 3.17 | $SnO_2$ | Tetragonal | 03-1116 | 27 |
| 9 | 500 | 6 | 4.72 | 3.17 | $SnO_2$ | Tetragonal | 03-1116 | 29 |
| 10 | 500 | 10 | 4.72 | 3.17 | $SnO_2$ | Tetragonal | 03-1116 | 38 |

maximum transparency is obtainable after annealing of thin films at 500 °C under $O_2$ atmosphere for 10 h.

## 3 Results and Discussion

### 3.1 XRD analysis

X-ray diffraction measurements were carried out on the films deposited onto glass substrates to identify the structure, crystallite size and the phase formation of tin oxide thin films by XRD. Figure 4(a-e) represents the XRD patterns of tin oxide thin films deposited in the vacuum of the order of $10^{-6}$ mbar and annealed at different temperatures (150 °C and 200 °C) for different time periods (2 h and 5 h) under high purity oxygen gas atmosphere. Figure 4(a) represents the XRD pattern of the as deposited thin film. All the peaks with orientations (200), (101),

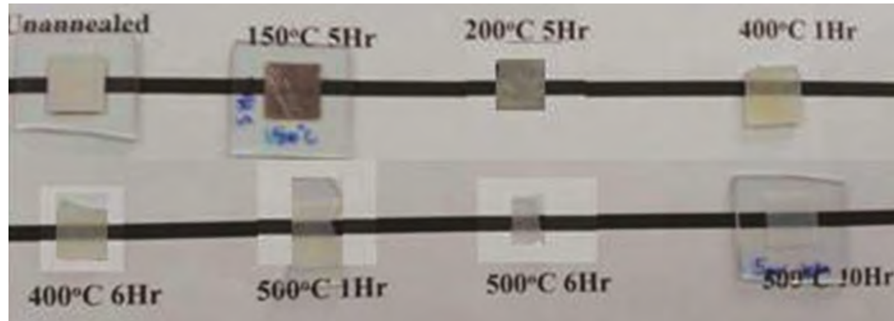


Fig. 3 — Effect of annealing conditions on the transparency of the $SnO_2$ thin films

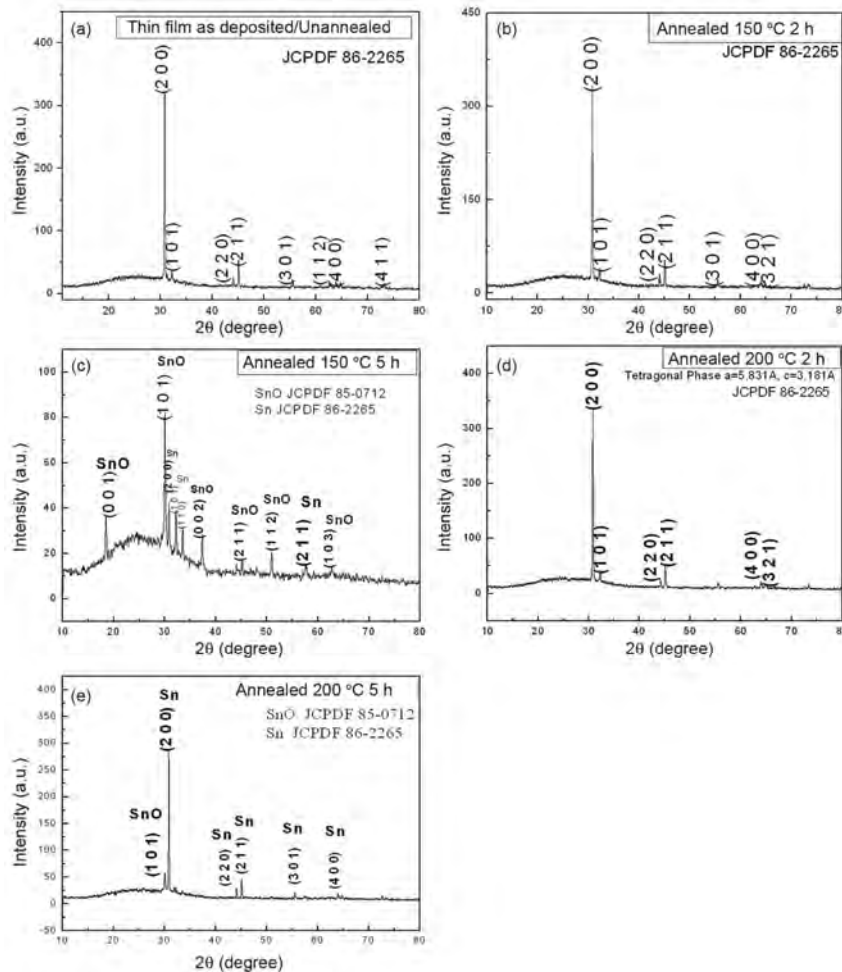


Fig. 4 — XRD pattern of tin and tin oxide thin films annealed at different temperature and time

(220), (211) and (301) in this spectra belongs to single phase of Sn (JCPDF No. 86-2265) having lattice parameters (*a* = 5.831 Å and *c* = 3.181 Å) with tetragonal structure. On annealing these films at 150 °C and 200 °C for 2 h indicates the formation of Sn phase only, i.e., SnO/$SnO_2$ phase is not formed. However when these films were annealed at 150 °C and 200 °C for 5 h, some reflections of SnO have also been observed as shown in Fig. 4(c and e). Reflections of SnO as shown Fig. 4(c) are in good agreement with the JCPDF No. 85-0712 having lattice parameters (*a* =3.796 Å and *c* = 4.816 Å) with tetragonal structure.

As deposited Sn thin films were further annealed at 400 °C and 500 °C for different time periods under oxygen atmosphere in order to synthesize good quality single phase $SnO_2$ thin films. Figure 5 represents the XRD patterns of $SnO_2$ thin films annealed at different temperature and time periods. It is revealed from the patterns that the films annealed at 400 °C for 1 h indicated the formation of single phase $SnO_2$ having tetragonal structure. All the peaks with orientations (110), (101), (200), and (211) in this spectra belongs to single phase of $SnO_2$ (JCPDF 03-1116) having lattice parameters (*a* = 4.72 Å and *c* = 3.17 Å). When these films were further annealed at 400 °C for 6 h and at 500 °C for 1 h, this resulted in the presence of same reflections at 2θ degree having similar intensities. However on annealing at 500 °C for 6 h and 10 h, a sharp oriented growth have been observed along (101) plane. Apart from the above, growth along (202) plane was also noticed at 500 °C for 10 h annealing, as depicted in Fig. 5. The detailed study of tin oxide thin films by using Bragg's equation suggested the formation of single phase $SnO_2$ having tetragonal structure.

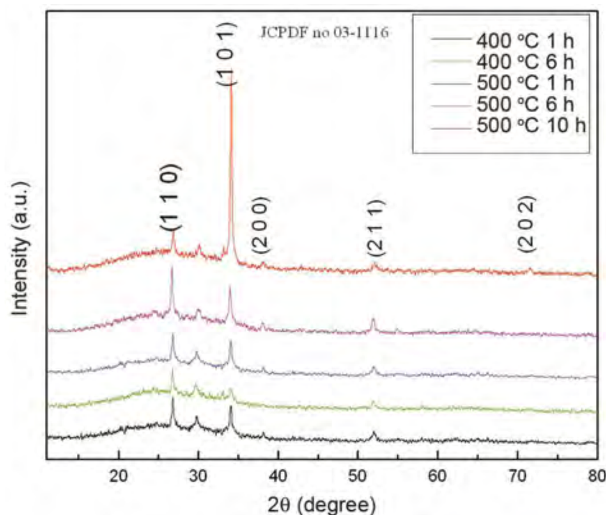


Fig. 5 — XRD patterns of $SnO_2$ thin films annealed at different temperature and time under $O_2$ atmosphere

It is known that on scattering of X-rays from a crystal lattice the condition for maximum intensity contained in Bragg's law above allow us to calculate details about the crystal structure, or if the crystal structure is known, to determine the wavelength of the X-rays incident upon the crystal:

$$2d\sin\theta = n\lambda \quad \dots (1)$$

where, *d* is interplaner spacing, θ is incident angle and λ is wavelength of X-rays. The average crystallite size (*D*) was estimated using the Scherrer equation as given below:

$$D = 0.9\lambda/\beta\cos\theta \quad \dots (2)$$

where *D* is the crystallite size, λ is the X-ray wavelength, β is the full width at half maximum of the diffraction peak, and θ is the Bragg diffraction angle of the diffraction peaks. The average crystallite size is mentioned in Table 1.

### 3.2 SIMS analysis

To study the elemental distribution in the as deposited tin thin films under the vacuum of the order of $10^{-6}$ mbar at room temperature, we have performed the depth profile experiment using a time of flight secondary ion mass spectrometer (TOF-SIMS) of ION-TOF GmBH, Germany. The secondary ions were created by bombarding pulsed primary ions from a 25 keV Bi liquid-metal ion gun (LMIG). The Bi current was fixed at 1.2 pA. The primary ion dose density was kept at $5\times10^{13}$ ions/cm$^2$ for tin oxide thin film. The source of 1 keV Cs was used to sputter out materials from the sample surface in order to analyze the depth. The sputtering was done on 250×250 μm$^2$ raster area while the analysis was done on 72×72 μm$^2$ area. The overall depth resolution was ~1 nm. The experiment was performed under ultra high vacuum condition with $5\times10^{-8}$ Pa pressure. Depth profile of Sn thin film deposited at room temperature (RT) in vacuum of the order of $10^{-6}$ mbar onto glass substrate was recorded by using TOF-SIMS.

Figure 6 depicts the typical SIMS pattern of the as deposited Sn film revealing the presence of SnO and $SnO_2$ phase along with tin. SIMS pattern also indicate that the film is non uniform in particular sputtered area. This is also to mention here that although the film is deposited under high vacuum conditions, even

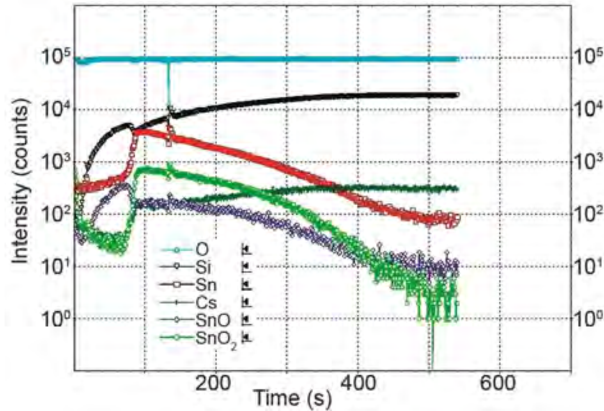


Fig. 6 — Depth profile of Sn thin film deposited under vacuum of the order of $10^{-6}$ mbar recorded under TOF-SIMS

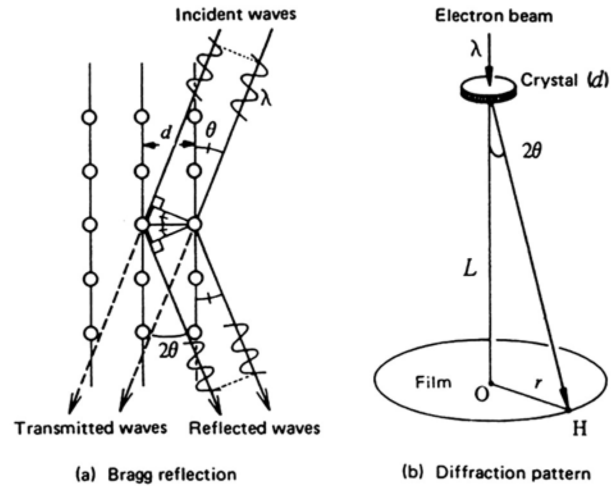


Fig. 7 — Schematic diagram of electron diffraction formation

though very little amount of SnO and $SnO_2$ is present as depicted in SIMS data. However we could not get the reflection of SnO and $SnO_2$ in the XRD pattern of the thin film deposited at RT (Fig. 1 (a)) which may be due to the presence of very low percentage of SnO and $SnO_2$ that could not be detected by X-ray diffractometer.

**3.3 Evolution of microstructure and reciprocal space analysis**

It is well known that electron beam interacts with substances to a far greater extent than in the case of X-rays. In other words the scattering power (diffraction wave amplitude/ incident wave amplitude) of electron beams is far greater ($10^6$ times or more) than that of X-rays. As a result small specimen is able to yield clear diffraction patterns.

That is to state that the film with a thickness of 50 nm or less can be effectively studied by electron beam diffraction. Furthermore electron is used to estimate the orientation of the crystal and the size and shape of the crystallite from the shape and structure of the pattern. When incident electron waves are scattered by the atoms in a substance, the wave expands spherically from the center of the atom. Moreover, when the specimen is in the crystalline state, having a regular three dimensional arrangement of atoms, a constant phase relationship exists between the waves emitted from the respective atoms.

These waves travel in one direction only and are mutually coherent. This is known as “Bragg’s reflection”. The electron waves are reflected by the atomic net planes. If the path difference, $2d\sin\theta$ (shown by the thick lines in the Fig. 7) is equal to $n\lambda$, where $n$ is an integer, and $\lambda$ is the wavelength, the waves reflected at successive planes will be in phase. Thus, equation $2d\sin\theta = n\lambda$ is obtained.

When an electron microscope is used as an electron diffraction apparatus, the equation changes to $d.2\theta = \lambda$:

$$\lambda/d = 2\theta \quad \ldots (3)$$

where $n = 1$ and $\sin\theta \approx \theta$, Bragg angle for high velocity electron beam is very small. Here in Fig. 7, O is the centre spot, H is the diffraction spot (or a point in the ring), and $L$ is the distance between the crystal and the film (camera length), $r$ is the distance between O and H can be express as follows. Now from diffraction pattern $r/\mathrm{L} = \tan 2\theta$, as $\tan 2\theta \approx 2\theta$, when $\theta$ is very small:

$$r/L = 2\theta \quad \ldots (4)$$

From Eqs (3) and (4),

$$rd = L\lambda \quad \ldots (5)$$

Knowing the values of $r$, $L$ and $\lambda$, we can calculate interplanar spacing $d$, where $L\lambda$ is known as camera constant.

Microstructural features associated with Sn thin film deposited in the vacuum of the order of $10^{-6}$ mbar recorded under TEM is shown in Fig. 8(a). From the TEM micrograph, it is observed that the film consists of randomly oriented fine crystallites of size 30-60 nm having polyhedral shape. Corresponding selected area electron diffraction ring pattern (SAEDP) of thin film is shown in Fig. 8(b) depicting a polycrystalline nature of the material. Diffraction spots on the rings indicate that the polycrystalline grain growth has taken place. Detailed analysis of the electron diffraction pattern of Sn thin

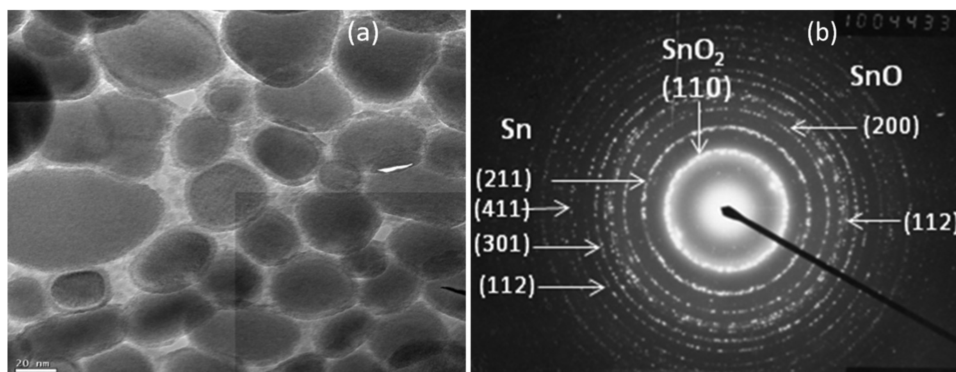


Fig. 8 — TEM image and the selected area electron diffraction (SAED) pattern of the as deposited Sn film

Table 2 — Electron diffraction ring pattern analysis of Sn thin film deposited under vacuum of the order of $10^{-6}$ mbar showing the presence of Sn and SnO phase; $L$ = 100 cm, λ = 0.0316 Å at accelerating voltage of 160 kV

| S. No. | Diameter of ring $r$ (cm) | Intensity of the ring | Observed spacing $d$ (Å) | $d$-spacing as per JCPDF data (Å) | ($hkl$) planes of Sn | ($hkl$) planes of SnO | ($hkl$) planes of $SnO_2$ |
|---|---|---|---|---|---|---|---|
| 1 | 1.92 | Strong | 3.291 | 3.300 | | | (110) |
| 2 | 3.25 | Strong | 1.956 | 2.016 | (211) | | |
| 3 | 3.40 | Point medium | 1.858 | 1.898 | | (200) | |
| 4 | 3.75 | Medium | 1.689 | 1.792 | | (112) | |
| 5 | 3.80 | Medium | 1.654 | 1.658 | (301) | | |
| 6 | 4.15 | Medium | 1.522 | 1.484 | (112) | | |
| 7 | 4.90 | Weak | 1.289 | 1.292 | (411) | | |

films deposited at room temperature (RT) has been done and summarized in Table 2. Seven clearly visible rings as marked in the SAEDP starting from centre of the electron diffraction pattern were thoroughly analysed in order to identify the phases present in the Sn tin thin films deposited at room temperature in the vacuum of $6\times10^{-6}$ mbar.

Analysis of SAEDP clearly indicates the presence of SnO and $SnO_2$ phases having tetragonal structure along with presence of unreacted Sn phase. The results are found to be in good agreement with JCPDF file No 85-0712, JCPDF file No. 03-116 and JCPDF No. 86-2265, respectively. Presence of SnO and $SnO_2$ along with the Sn phase was also revealed in the surface analysis carried out by using TOF-SIMS as shown in spectra (Fig. 6). This suggests that although the films were synthesized in high vacuum conditions but still some oxygen exists in the evaporation chamber which may be responsible to react with Sn to form SnO and $SnO_2$ phase during the synthesis of the thin film.

**3.4 Surface morphology analysis of thin films**

Surface morphology of the as deposited and annealed tin oxide thin films were analyzed by using scanning electron microscope (SEM). Films were thoroughly scanned under SEM and images were recorded at suitable magnifications as shown in Fig. 9(a-c). Surface microstructure of thin films exhibits that in as grown condition, films consist of irregular shape and elongated grains scattered in different directions uniformly. The particle size of Sn is close to 500 nm. Growth of tin oxide films annealed at 400 °C for 6 h has occurred in both lateral and longitudinal directions, as shown in Fig. 9(b). The size of the particles is found to be increased. However the crystallites of tin oxide start nucleation on the top surfaces of the particles with an average size of around 25 nm size. The crystallite sizes are also calculated by Scherrer equation (Table 1). After annealing the films in oxygen atmosphere at 500 °C for 6 h, the cracks in the thin films are appeared due to the difference of linear thermal expansion coefficient of substrate and tin oxide thin film. The magnified image of crack is shown in the inset of Fig. 9(c). Evolution of ultra-fine grains at high temperature (500 °C) clearly reveals the process of re-crystallization in as-deposited and subsequently annealed films.

**3.5 Atomic force microscopy analysis**

AFM scans were performed using a multimode V; make Veeco instrument in contact mode with NP 20

tips. The scan area was taken 3 µm×3 µm. AFM micrographs of the nano-crystalline tin oxide thin films show that the shape, size and arrangements of the grains are different for the films deposited under different process conditions. Figure 10(a-g) shows the AFM images of all the tin oxide films. Figure 10(a) represents the top view of AFM images of the as deposited Sn film. A detailed investigation of AFM image shows that film has randomly oriented grains with average grain size about 600 nm. The measured RMS roughness of the thin films is found to be ~37 nm with an average height of the grains ~130 nm. Figure 10(b-d) represents the AFM image of the surface of thin films annealed in the presence of oxygen at 400 °C for 1, 5 and 6 h. Figure 10(e-g) shows the surface topography of the films annealed at 500 °C for 1, 6 and 10 h. Tin oxide films annealed at 400 °C show the aggregated grains size which

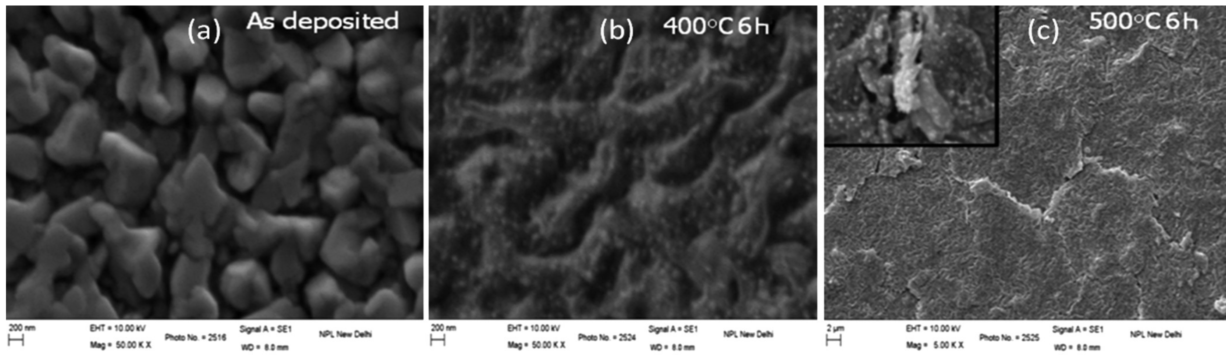


Fig. 9 — SEM micrographs of (a) as deposited Sn film, (b) film annealed at 400 °C for 6 h and (c) film annealed at 500 °C for 6 h and inset shows the magnified view of image depicting re-crystallization

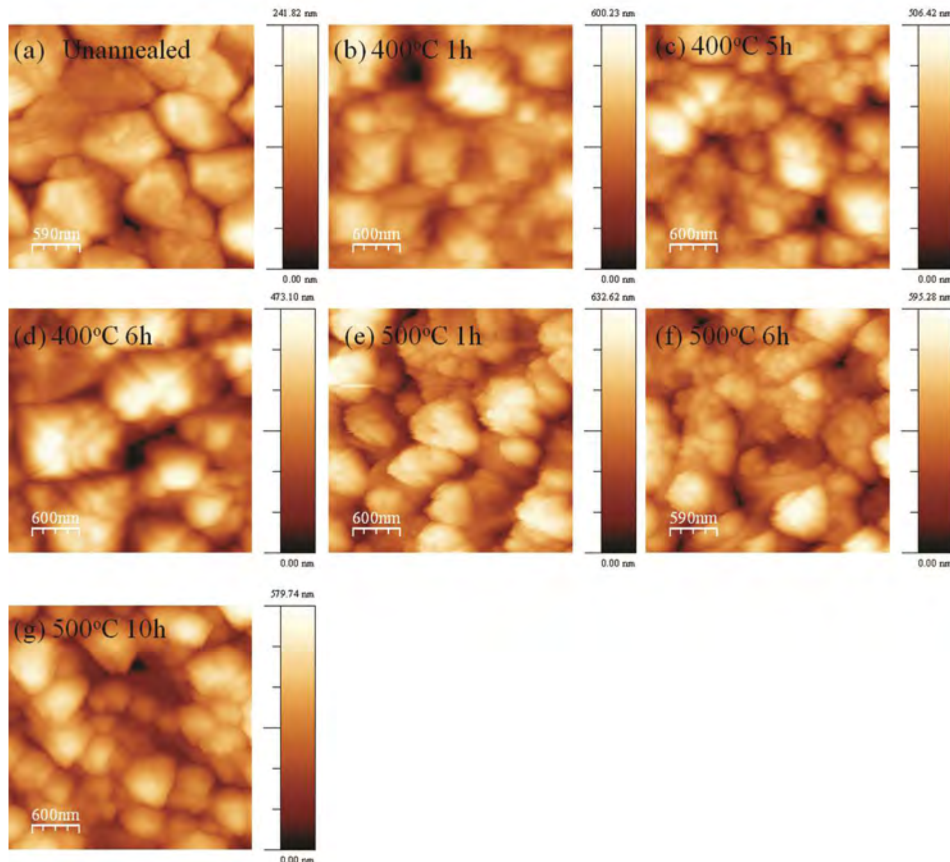


Fig. 10 — AFM micrographs of (a) as deposited Sn film, (b) film annealed at 400 °C for 1 h, (c) film annealed at 400 °C for 5 h, (d) film annealed at 400 °C for 6 h, (e) film annealed at 500 °C for 1 h, (f) film annealed at 500 °C for 6 h and (g) film annealed at 500 °C for 10 h

Table 3 — Summary of RMS roughness and average height of tin oxide thin films processed under different conditions

| S. No. | Sample | RMS roughness (nm) | Average height (nm) |
|---|---|---|---|
| 1 | As Deposited | 37 | 130 |
| 2 | 400 °C; 1 h | 94 | 321 |
| 3 | 400 °C; 5 h | 91 | 265 |
| 4 | 400 °C; 6 h | 85 | 234 |
| 5 | 500 °C; 1 h | 118 | 329 |
| 6 | 500 °C; 6 h | 100 | 290 |
| 7 | 500 °C; 10 h | 96 | 270 |

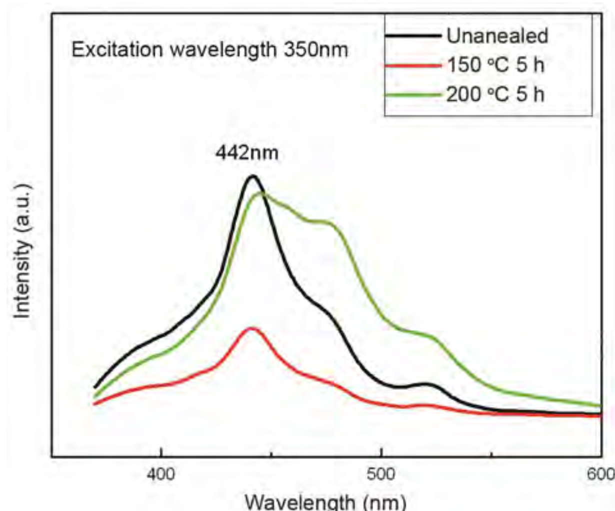


Fig. 11 — Photoluminescence spectra of the films as deposited, annealed at 150 °C and 200 °C for 5 h

decreases with the increase of annealing time. The measured value of RMS roughness and average height of thin films decreases with annealing time. Tin oxide films annealed at 500 °C show that grain size, RMS roughness and average height of the grains are decreasing with increasing annealing time as given in the Table 3.

**3.6 Photoluminescence**

Photoluminescence measurements were carried on tin oxide thin films by using PL spectrometer (model Elmer Perkin model LS 55) in the emission range of 370 to 600 nm at an excitation wavelength of 350 nm for the films deposited at RT, annealed at 150 °C and 200 °C for 5 h (Fig. 11). The presence of emission peak at 442 nm is found to be of SnO and $SnO_2$ in the as deposited as well as annealed at 150 °C and 200 °C for 5 h. Existence of SnO and $SnO_2$ at these conditions are in good agreement with the phase interpretations in electron diffraction and SIMS analyses. Figure 12 depicts the PL spectra of $SnO_2$ thin films annealed at 400 °C and 500 °C for 1 h, 6 h and 10 h at the excitation wavelength of 300 nm in the emission range of 400 to 550 nm.

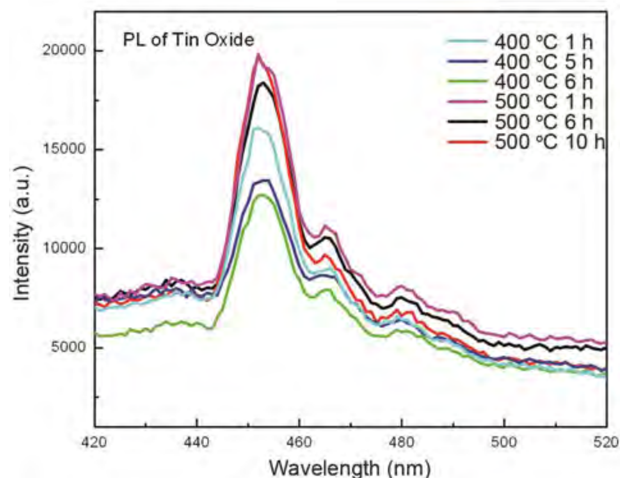


Fig. 12 — PL spectra of $SnO_2$ thin films annealed at 400 °C and 500 °C at different time periods

From the PL spectra as shown in Fig. 11, it is observed that there is one emission peak centred at wavelength 442 nm for the films deposited at RT, annealed at 150 °C and 200 °C for 5 h. The optical band gap was estimated from this PL data and found to be 2.81 eV. For the emission peak at 452 nm of $SnO_2$ thin films annealed at 400 °C and 500 °C for 1 h, 6 h and 10 h (Fig. 12), the band gap was found to be 2.75 eV.

## 4 Conclusions

Tin oxide thin films synthesized by vacuum evaporation technique and further annealed at different temperatures for different periods of time under the oxygen atmosphere has revealed very interesting features. It is observed that annealing at 400 °C and 500 °C for 1 h, 6 h and 10 h under oxygen atmosphere has resulted in the formation of good quality single phase $SnO_2$ thin films. It is observed that Sn thin film annealed at 500 °C for 10 h revealed the highest transparency. Detailed analysis of electron diffraction pattern, pholuminesence spectra and SIMS data exhibited that even at room temperature deposition under high vacuum conditions, SnO and $SnO_2$ phases coexist. It is also noted that annealing temperature and time play important roles for the reaction of Sn and $O_2$ in nucleation and growth process to result a single phase $SnO_2$ thin films. Evolution of ultra-fine grains at high temperature clearly reveals the process of re-crystallization in as-

deposited and subsequently annealed films. Further work is in progress to carry out the resistivity measurements of these thin films in various gases atmosphere in order to assess the material for various gas sensors.

**Acknowledgments**

One of the authors PJ is thankful to Council of Scientific and Industrial Research (CSIR-India) for providing the fellowship under which this research work is being carried out. We would also like to thank Director NPL India for providing the necessary experimental facilities to carry out our research work.

## References

1 Sundaram K B & Bhagavat G K, *J Phys D*, 14 (1981) 921.
2 Chung J H, Choe Y S & Kim D S, *Thin Solid Films*, 349 (1999) 126.
3 Sanon G, Rup R & Mansingh A, *Phys Rev B*, 44 (1991) 5672.
4 Contreras M, Romero M, To B, Hasoon F, Noufi R, Ward S & Ramanathan K, *Thin Solid films*, 403-404 (2002) 204.
5 Davis A, Vaccaro K, Dauplaise H, Waters W & Lorenzo J, *J Electrochem Soc*, 146 (1999) 1046.
6 Galan O V, Quiebras J X, Hernandez J A, Puente G C, Orea A C, Alvarez J M, Bedoya J C, Ruiz C & Bermudez V, *Semicond Sci Technol*, 21 (2006) 76.
7 Llieva M, Malinovska D D, Ranguelov B & Markov I, *J Phys Condens Matter*, 11 (1999) 10025.
8 Manea E, Budianu E, Podaru M P, Popescu A, Cernica I, Babarada F & Parvulescu C C, *Rom J Inf Sci Technol*, 10 (2007) 25.
9 Timonah N S, Chunhui Y & Liang S, *Mater Sci Semicond Proc*, 13 (2010) 125.
10 Changhyun J, Kyungjoon B, Sunghoon P, Hyoun W K, Wan Il & Chongmu L, *Sol State Commun*, 150 (2010) 1812.
11 Partridge G, Field M R, Peng J L, Sadek A Z, Zadeh K K, Plessis J D & McCulloch D G, *Nanotechnol*, 19(12) (2008) 5504.
12 Serin T, Serin N, Karadeniz S, Sar H, luoglu N T & Pakma O, *J Non-Cryst Solids*, 352 (2006) 209.
13 Delgado F P, Yoshida M M, Antunez W, Hernandez J G, Vorobiev Y V & Prokhorov E, *Thin Solid Films*, 516 (2008) 1104.
14 Takeya O, Takayoshi O, Dong L S & Shizuo F, *Physica Status Solidi*, 8(2) (2011) 540.
15 Jain P, Singh S, Siddqui A M & Srivastava A K, *Adv Sci Eng Med*, 4 (2012) 230.